Accepted Manuscript

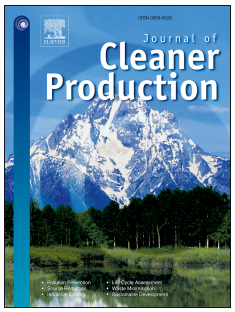

Next frontiers in cleaner synthesis: 3D printed graphene-supported CeZrLa mixed-oxide nanocatalyst for CO_2 utilisation and direct propylene carbonate production

Vesna Middelkoop, Thomas Slater, Mihaela Florea, Florentina Nea□u, Simge Danaci, Victor Onyenkeadi, Katrien Boonen, Basudeb Saha, Ioan-Alexandru Baragau, Suela Kellici

PII: S0959-6526(18)33981-7

DOI: https://doi.org/10.1016/j.jclepro.2018.12.274

Reference: JCLP 15332

To appear in: *Journal of Cleaner Production*

Received Date: 15 May 2018

Revised Date: 21 December 2018

Accepted Date: 25 December 2018

Please cite this article as: Middelkoop V, Slater T, Florea M, Nea□u F, Danaci S, Onyenkeadi V, Boonen K, Saha B, Baragau I-A, Kellici S, Next frontiers in cleaner synthesis: 3D printed graphene-supported CeZrLa mixed-oxide nanocatalyst for CO_2 utilisation and direct propylene carbonate production, *Journal of Cleaner Production* (2019), doi: https://doi.org/10.1016/j.jclepro.2018.12.274.

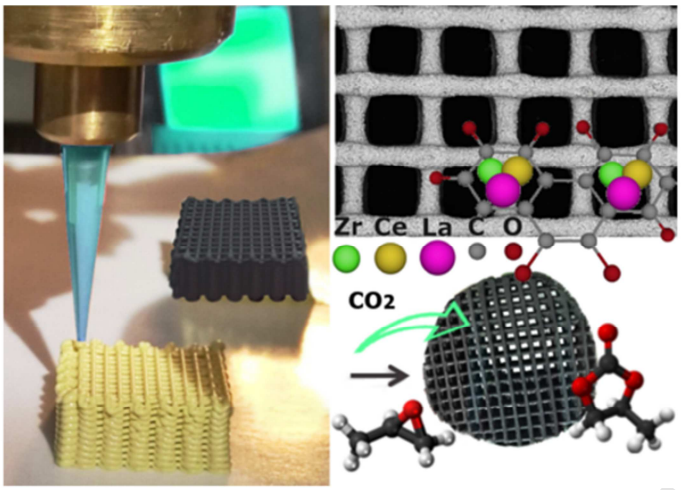

count: 6756

Next frontiers in cleaner synthesis: 3D printed graphene-supported CeZrLa mixed-oxide nanocatalyst for CO_2 utilisation and direct propylene carbonate production

Vesna Middelkoop,[†,*] Thomas Slater,[‖] Mihaela Florea,[⊥] Florentina Neațu,[⊥] Simge Danaci,[†,‡,§] Victor Onyenkeadi,[#] Katrien Boonen,[†] Basudeb Saha,[#] Ioan-Alexandru Baragau,[#] Suela Kellici,[#,*]

[†] Flemish Institute for Technological Research - VITO, Boeretang 200, B-2400 Mol, Belgium

[‖] School of Materials, University of Manchester, Manchester, M13 9PL, UK

[⊥] Laboratory of Multifunctional Materials and Structures, National Institute of Materials Physics, Atomistilor Str. 405A, 077125 Magurele, Romania

[‡] Liten/DTBH/SCTR/LER, CEA Grenoble, 17 rue des Martyrs, 38054 Grenoble, France

[§] LEGI, UJF-Grenoble 1/Grenoble-INP/CNRS, BP53, Grenoble F-38051, France

[#] School of Engineering, London South Bank University, 103 Borough Road, London SE1 OAA, UK

Corresponding authors

*E-mail: vesna.middelkoop@vito.be; Tel.: +3214335737.

*E-mail: kellicis@lsbu.ac.uk; Tel.: +442078157983.

KEYWORDS: ceria-lanthana-zirconia graphene oxide; nanocomposite catalyst; continuous hydrothermal flow synthesis; direct-write 3D printing; propylene carbonate, CO_2 utilisation; green synthesis

ABSTRACT:

A rapidly-growing 3D printing technology is innovatively employed for the manufacture of a new class of heterogenous catalysts for the conversion of CO_2 into industrially relevant chemicals such as cyclic carbonates. For the first time, directly printed graphene-based 3D structured nanocatalysts have been developed combining the exceptional properties of graphene and active CeZrLa mixed-oxide nanoparticles. It constitutes a significant advance on previous attempts at 3D printing graphene inks in that it does not merely explore the printability itself, but enhances the efficiency of industrially relevant reactions, such as CO_2 utilisation for direct propylene carbonate (PC) production in the absence of organic solvents. In comparison to the starting powder, 3D printed GO-supported CeZeLa catalysts showed improved activity with higher conversion and no noticeable change in selectivity. This can be attributed to the spatially uniform distribution of nanoparticles over the 2D and 3D surfaces, and the larger surface area and pore volume of the printed structures. 3D printed GO-supported CeZeLa catalysts compared to unsupported 3D printed samples exhibited higher selectivity and yield owing to the great number of new weak acid sites appearing in the supported sample, as observed by NH3-TPD analysis. In addition, the catalyst's facile separation from the product has the capacity to massively reduce materials and operating costs resulting in increased sustainability. It convincingly shows the

potential of these printing technologies in revolutionising the way catalysts and catalytic reactors are designed in the general quest for clean technologies and greener chemistry.

1. Introduction

In response to the pressing need for the decarbonisation of industry sectors, there is increasing interest in developing new technologies for deploying captured CO_2 as a building block in commercially viable production processes and green catalysis.[1,2] This work takes concrete steps towards realising the potential of CO_2 utilisation by interfacing CO_2 utilisation technologies with emerging manufacturing technologies such as 3D printing to advance the frontier of green catalysis. The synthesis of valuable chemicals such as cyclic carbonates from CO_2 is a highly desirable environmentally-friendly alternative to conventional synthesis methods that involve the use of toxic solvents and species, multiple steps, including homogeneous catalysts, and product separation.

Propylene carbonate is an industrially relevant compound with applications in the chemical, pharmaceutical, automobile and electronic industries. Solvent-free heterogeneous catalytic systems are considered more efficient, economically feasible and a greener synthetic route for valuable chemical synthesis. Metal oxide catalysts such as CeO_2, ZnO, Zr_2O, La_2O_3, and in particular their graphene oxide (GO)-supported nano-composites in powder, have already been identified by the authors and other researchers as suitable for the conversion reaction of CO_2 and propylene oxide (PO) to propylene carbonate (PC).[3,4] An extensive overview of major developments in the field of catalysis and cyclic carbonate synthesis from 1969 to date has been provided by North et al. The most important groups of catalyst are homogeneous and heterogeneous catalysts, catalysts in the presence of ionic liquids[5] as both solvents and catalysts, and their combination with metal salts, organo-catalysts, metal oxides, and metal complexes[6]. Only a small number of catalysts exhibit good catalytic performance especially under ambient temperature and atmospheric pressure, as high temperature and/or high pressure tend to accelerate cyclic carbonate synthesis.[7] This work employs for the first time high-performance, heterogeneous, easy-separable 3D printed GO-supported as well as unsupported CeZrLa catalysts for the efficient conversion of CO_2 to PC in a batch reaction to demonstrate the use of innovative structured catalyst and reactor concepts for added value chemicals in the absence of organic solvents.

The 2D sheets of graphene, when incorporated into monolithic 3D bulk assemblies, exhibit extraordinary intrinsic properties: high surface area, chemical stability, excellent electrical and thermal conductivity. As summarised in a review by Tang et al., graphene-related nanomaterials are suitable for a wide range of applications including energy storage and generation (e.g. electrodes for lithium ion batteries, supercapacitors, solar and fuel cells), chemical and biochemical sensors, optical devices and high speed electronics, as well as CO_2 conversion technologies (e.g. catalysts and absorbers).[8] In the past three years, there have been a number of reports of 3D printing successes of graphene oxide aerogels into microlattices based on homogenously dispersed graphene materials in polymer matrices.[9,10,11,12,13]

The simplicity of the preparation and manufacturing methods lies in the fact that it does not require additional steps (such as the incorporation of inorganic binders, introduction of

solvents and organic solvent baths, gelation through organic sol–gel chemistry, etching in acid solutions, supercritical drying or a freeze-casting step to remove the solvent/water) in order to preserve the 3D architecture, unlike most of the other fabrication methods of 3D printed GO structures.[14,15] The techniques for 3D printing-enabled chemical reactor design are in their infancy with a few very recent notable examples of successful pioneering work, such as 3D printed α-Al_2O_3 for Biginelli and Hantzsch reactions;[16] Cu/Al_2O_3 catalyst for different Ullmann reactions[17]; 3D printed stainless steel supports coated by zeolite for methanol-to-olefin conversion[18]; Ni/Al_2O_3 coated 3D printed copper structures for CO_2 methanation[19] and directly printed carbon and zeolites structures for gas sweetening.[20] This work builds upon it and represents a leap forward in exploiting the properties of 3D printed architectures for well-controlled and adaptable catalytic reactor design.

2. Experimental

2.1 Materials Preparation

The starting powders (CeZrLa and CeZrLa/GO nanocomposites) were obtained by utilising an environmentally benign, rapid, single-step chemical synthesis route, Continuous Hydrothermal Flow Synthesis (CHFS) process, as previously described.[21] The process involves mixing (in a specially designed reactor) a flow of superheated water with a flow of water-soluble precursor(s) to give controlled, continuous and rapid synthesis (within seconds) of nanomaterials. This system offers a variety of instant controls (temperature, pressure, residence time, reactant concentration) that allows a high degree of tailoring/functionalisation of the 2D materials (oxidation, composition, surface area, etc.) to attain the desired properties.

The CHFS as-synthesised nanomaterials were prepared into ink formulations for 3D printing from the optimal polymer/powder ratio of 54 wt% of polymer (an aqueous solution of methyl cellulose) and 42 wt% of the nano-powder that were mixed with a small amount (4 wt%) of lubrication additive using a planetary centrifugal mixer (Thinky Mixer ARE-250). The printing suspensions were confirmed to exhibit non-Newtonian shear-thinning behaviour using a Haake-Mars rotational rheometer with a plate-to-plate configuration.

Both GO-supported and unsupported nanocomposite lattices were fabricated layer by layer by the direct co-extrusion of a viscous nanocomposite paste through a syringe and a nozzle mounted on an x,y,z stage in order to construct arrays of definite geometrical patterns and morphology with excellent reproducibility. The rheologies of the printing suspensions combined with an array of printing parameters (such as the speed of stage of about 2000 mm/min, the syringe pump rate in a range of 400-600 µl/min and the size of the nozzle of 400-800 µm) are key factors in making precise regular constructs of a specific pre-programmed pattern and geometry. In order to obtain self-supporting stacked layers of printed fibers that maintain sufficient mechanical integrity, they were gradually dried, first in a climate chamber, then in air over the course of several days, with subsequent heat-treatment in an inert gas at 500°C to remove the binder. Figure 1 shows a schematic illustration of the catalyst preparation process and the resulting structures mounted into the reactor. SEM images of a representative resulting 3D printed structures are shown in Figure 4 and Figure S6 in Supporting Material.

2.2. Materials characterisation and catalytic experiments

Thermogravimetric data were obtained by heating the fresh samples at a heating rate of 10°C min^{-1} in Helium using a Netzsch STA 449C instrument. Micro-structural parameters such as pore volume, pore size distribution and specific surface area were determined from the N_2 adsorption measurements using the Barrett-Joyner-Halenda (BJH) and the Brunauer-Emmett-Teller (BET) methods respectively for the printed samples, as well as the CeZrLa-GO sample after reaction using a Quantachrome Autosorb IQ instrument.

XRD measurements were conducted on a Philips/Panalytical X'Pert diffractometer (Cu Kα radiation) using a voltage of 40 kV and a current of 40 mA, at room temperature over a 2 to 100° 2θ range (with a step size of 0.04° and a time of 4 seconds per step). The temperature dependent XRD measurements were performed on a

Panalytical Empyrean with PIXEL3D detector, using Cobalt Kα radiation (λ = 1.790307 Å), a voltage of 40 kV and a current of 45 mA over a 5 to 120° 2θ range (with a step size of 0.01° and a step time of 45 seconds).
An FEI Talos F200A, equipped with Super-X detectors and operated at 200 kV, was used to acquire transmission electron microscope (TEM) images and selected area electron diffraction (SAED) patterns. Additionally, high angle annular dark field (HAADF) images and energy dispersive X-ray (EDX) spectrum images were acquired with this instrument employed as a scanning transmission electron microscope (STEM). An FEI Quanta 650 scanning electron microscope (SEM), equipped with an Oxford Instruments X-Max EDX detector, was used to obtain secondary electron images and EDX spectrum images.

Ammonia temperature programmed desorption (NH3-TPD) profiles for 3D printed CeZrLa and CeZrLa-GO material (see Table 3, and Figure 7) were obtained using a Porotec TPDRO1100 instrument equipped with a programmable temperature furnace and TCD detector. The experimental conditions were as follows: 0.10 g of sample was purged for 2 h with 20 mL/min He at 200 °C. Then, 5% NH_3/He was flushed for 10 min at 100 °C. This temperature is used to minimise physisorption of the ammonia or organic amines on the materials. The sample was then purged with 20 mL/min He at 100 °C for 2 h, in order to remove the weakly adsorbed species. After, under the same flow of He, the temperature was raised to 700 °C at 20 °C/min, and the desorbed products were analysed with a TC detector. The desorbed NH_3, expressed as µmols per gram of catalyst, was determined using a calibration curve.

X-ray photoelectron spectroscopy (XPS) measurements were performed at normal emission in an AXIS Ultra (Kratos) set up, using Al Kα monochromated radiation (hv= 1486.7 eV) of an X-ray gun, operating with 300 W (12 kV/25 mA) power. A flood gun with electron acceleration at 1 eV, and electron current of 100 lA, was used in order to avoid charge effects. A charge neutraliser was used for all samples for charge compensation. The instrument was calibrated with metallic gold at 83.96 eV (Au $4f_{7/}2$). The XPS spectra were fitted using a Voigt profile with individual inelastic background for each component. Taking into account the charging effect on the measured Binding Energies (BEs), the spectra were calibrated using the C1s line (BE = 284.6 eV, C-C $(CH)_n$ bonds) of the adsorbed hydrocarbon on the sample surface.

The direct synthesis of propylene carbonate (PC) using 3D printed catalysts was performed from the cycloaddition of carbon dioxide and propylene oxide (PO) in a Parr pressure reactor in the absence of any organic solvents. Catalytic tests have been performed on printed 3D CeZrLa-GO and 3D unsupported CeZrLa-samples. The reaction product was analysed with a Shimadzu GC-2014 gas chromatograph (GC) equipped with a capillary column with dimensions 30 m × 320 µm × 0.25 µm and a flame ionization detector (FID).

3. Results and discussion

The printed systems presented here comprise the (GO) nanocomposite powder dispersed in a matrix formed by a single organic polymer binder. The TGA-DTG analysis of the printed structures revealed that both nanocomposites are thermally stable after the temperature treatment, which involves burning off the polymer. From the TGA profiles (Supporting Information, Figure S1), changes in mass are measured as a function of temperature and time that correspond to the release of water from the 3D printed structures, followed by the polymer degradation in two stages. The profiles were found to have remarkably similar features for both the GO and non-GO containing samples.

An overview of the experimental conditions of the catalytic tests are shown in Table 1 and the comparison results of the printed catalyst testing are shown in Figures 2, S2 and S3. In an attempt to determine the effect of the experimental parameters and optimal process conditions a set of measurements was carried out on the printed GO-supported catalyst with varied parameters (firstly independently varying the catalyst loading and reaction time and then varying both parameters in one run). The effect of catalyst loading has already been studied by Adeleye et al. It was found that the catalyst to reactant ratio of 10 by weight was the most efficient for the

reaction.[4] The mass of the catalyst used in each of these runs was changed by cutting off an appropriate part of the printed cuboids. For each run the printed cuboids were machined into cylinders with a central bore for positioning the stirrer shaft.

It is evident from the repeat runs (see Figure 2) that the 3D printed CeZrLa-GO catalyst exhibited improved activity in comparison to the starting powder form, with higher conversion and no noticeable change in selectivity. This behaviour is supported by the surface area, which is higher for the 3D printed materials, meaning a greater accessibility to active catalytic sites, thus implicitly an increase in activity. The printed unsupported CeZrLa mixed oxide was used as a control sample for the printing parameters even though it was known to be showing less activity.[4] When comparing the printed GO-supported catalysts to the printed unsupported catalysts (Figure 2), the selectivity and yield were about 20% higher over the 3D printed GO-supported samples whereas the conversion levels were similar for both printed materials at a reaction temperature of 443 K, CO_2 pressure of 70 bar, catalyst loading of 10% (w/w), and reaction time of 20 h and a stirring speed of 100 rpm. As the number of actives sites is the same in the supported and unsupported sample, it is expected that the conversion does not change. Concerning the selectivity, it increases when the CeZrLa was supported on GO due to the fact that new active centres appear in the supported sample, as indicated further by NH_3-TPD analysis, which are probably responsible for the higher selectivity. The stirring speed for the printed GO-supported samples was varied between 100 and 350 rpm to study the influence of external mass transfer. For the 350 rpm stirring speed, the catalyst was found to achieve an almost negligible conversion increase compared to that with 100 rpm. There was no noticeable increase of PO conversion and PC yield beyond 350 rpm and hence 100 and 350 rpm have comparable activities, no external mass transfer occurs. For further experiments, 350 rpm was considered to be the optimum stirring speed. Under these conditions and 350 rpm the printed GO-supported catalyst exhibited a maximum yield of 89% with 96% selectivity of PC. The results compare well to the catalytic performance of commonly studied M-Al mixed oxide catalysts (where M represents Mg, Ca, Sr, and Ba) amongst which Zn-Mg-Al-oxide catalysts were found to have the highest activity, with PC yield and selectivity of 88.8% and 99.2% respectively, but only in the presence of triethylamine. In contrast, in the absence of triethylamine, the PC yield of Zn-Mg-Al dropped to 67.0% and selectivity to 95.9%, as Dai et al. report.[22] In comparison, not only does the 3D printed CeLaZe-GO oxide offer the advantage of catalysing cycloaddition reactions solvent-free, they also allow facile separation from the reaction product(s) by its own removal in one piece.

Furthermore, the geometry of the printed catalyst structures, i.e. the advantageous effect of the open multi-channel morphology, high surface area and a variety of fibre and channel dimensions is expected to affect the reaction if performed in a fixed-bed reactor, because a multi-channel pattern should favour the mixing dynamics. It should be noted that the potential of the patterned structures has yet to be fully exploited. In this study it has had a minor effect due to the reaction being performed in a stirred batch autoclave reactor and the geometry of the structured material would have a much more significant effect if it was employed in a continuous flow cell. However, the 3D structured catalyst offers many operational catalytic advantages over conventional approaches, offering materials with desirable properties including high surface area and pores, mechanical integrity, volumetric efficiency, improved mass and heat transfer and gas diffusion kinetics.

The specific surface area and porosity results are summarised in Table 2, showing that the fresh structured catalyst has a higher surface area and pore volume than the as-synthesised powder. Evident, but not significant, changes in the measured values of the porous structure of the used catalyst can be observed.

According to XRD data, there is no change in the phase of Ce, Zr and La oxides before and after reaction (Figure 3). For more detail on Rietveld analysis of the temperature-dependent and spent catalyst data see Supporting Information, Tables S2 and S3 and Figure S5).

While it is particularly challenging to differentiate between tetragonal and cubic phases of zirconia using XRD[23], the two phases can be distinguished through the presence of a (102) ring in selected area electron diffraction (see Figure 5a).[24] Here, SAED patterns do not show a (102) ring, indicating that the predominant phase is cubic zirconia, rather than the tetragonal phase. HRTEM images of nanoparticles supported the identification of cubic zirconia in samples both with and without GO included, in addition to a sample of used catalyst including GO (Figure 5b-c). The HRTEM images showed that there is no significant change in the populations of particles (65-79 particles for each sample, see Table 2). For the calcined 3D printed samples the HRTEM analysis showed the mean and standard deviation of the particle size distribution of 9.4 nm and 1.5 nm respectively. The (average) size of the nanoparticles estimated from the XRD patterns obtained with different instruments and at different conditions (various calcination temperatures and environments, N_2, He and air)_has been found to vary within the range of 5.2±0.6 to 7.9±0.6 (see Table S3 in Supplementary Information for further details on the particle size, calculated from the Scherrer equation from the four main corresponding diffraction peaks, (111), (200), (220) and (311) at 2θ positions of 29.8°, 34.5°, 49.7° and 59.0° respectively). It should be noted that XRD is commonly reported in the literature as limited albeit indicatory when characterising very small (nano)particles. Hence, XRD has been used in this work primarily to identify the phases present in the 3D printed samples and the particle size results serve as an indication (rather than absolute size) for cross-correlation with the particle size analysis by HRTEM. The results on particle size are, not surprisingly, not identical (with the values outside the error limits) and only in agreement to a certain extent (within the error limits between 7.9 and 8.5 nm). As widely acknowledged in the literature this is due to the fundamentally different nature of the HRTEM and XRD measurements: the HRTEM results present two-dimensional projections of the individual nanoparticles within the sample, expressed as the mean diameter and standard deviation while the XRD results are indirectly derived from the bulk/volume (of the so-called mean scattering domain size) via the Scherrer equation.

Energy dispersive X-ray (EDX) spectroscopic mapping in both the SEM and STEM was undertaken (Figure 5d and 5e). SEM-EDX mapping revealed that Zr, Ce and La were distributed homogeneously within the printed structures on a macroscopic scale for samples both with and without GO. STEM-EDX of clusters of individual nanoparticles confirmed the results of the diffraction data, that all nanoparticles appeared to be zirconia doped with cerium and lanthanum, rather than individual particles of zirconia, ceria and lanthana. For further details on microstructure and particle size see Supplementary Information, Figures S6, and S7 (for SEM, TEM and EDX analysis), along with Figures S4 (for pore volume and size distribution obtained from N_2 adsorption–desorption) and Table S3 (for particle size calculated from XRD data).

NH_3-TPD studies were performed to assess the acidic properties of the catalysts. The recorded NH_3-TPD profiles are presented in Figure 6 and the calculated amount of desorbed NH_3 (cm^3 STP/g) are presented in Table 3. The studied samples clearly show three distinct regions that can be attributed to weak, medium, and strong acid sites, and were assigned to the peaks of NH_3-TPD profiles at temperatures lower than 350 °C, between 350 and 500 °C, and above 500 °C, respectively.[25] The total uptake of ammonia was higher for the sample supported on GO, which also presented a higher number of weak and medium acid sites, that can be assigned to the GO.[26] Usually, the weak acid sites in GO are found at ~240 °C. [26] In the CeZrLa-GO samples, new weaker acid sites were observed (170 °C), probably due to the interaction between CeZrLa and GO. Also, the results can be related to Brønsted or Lewis sites.[25] Therefore, the low-temperature peak could be assigned to ammonia coordinated to Lewis acid sites, which desorb at temperatures around 200 °C, while the high-temperature peak corresponds to Brønsted-bonded ammonium, which is more thermally stable and desorbs later.[27,28] If we take this into account, we can observe that both samples present the same number of Brønsted acid sites (NH_3 uptake from 400 and 525°C) well known as accelerators for the cycloaddition of carbon dioxide and propylene oxide[29] and, indeed, the conversion for both samples is almost the same. The presence of a great number of new weak

acid sites in the GO supported sample can be correlated with the change in selectivity observed for supported and unsupported sample.

The full-survey-scan XPS spectra confirm the presence of La, Ce, Zr, C and O as can be seen from Figure 7. As we previously reported the hydrothermally treated precursor graphene oxide exhibited significantly reduced peak intensities of the oxygen-containing functional groups (epoxide, carboxyl and hydroxyl).[4] Since XPS is a surface sensitive technique (with a sampling depth of 2 to 10 nm), this observation can be interpreted as the effect of CeZrLa phase migration to the surface which is also consistent with a change in colour of the sample that occurred during the thermal treatment. The 3D printing of the GO-supported and unsupported structures preserved the character of the powder in terms of its chemical composition, as revealed by the XRD analysis.

Deconvolution of the XPS C1*s* peak shows a predominant component at a binding energy of 284.6 eV attributed to sp^2 carbon hybridisation, accompanied by other components in lower proportions assigned to C-OH (component appearing at 286.5 eV) and C-OOH (component appearing at 288.6 eV). In addition weak and broad K2p signals can be identified (see Figure 7b). The XPS high resolution spectra of Ce3d, O1s, Zr3d and La3d for both CeZrLa and CeZrLa-GO samples are displayed in Figure 7c-f. CeZrLa and CeZrLa-GO have similar spectra confirming that the CeZrLa phase was neither modified by the deposition method nor by the printing process and thermal treatment. According to the literature on Ce 3d spectra (Figure 7c), five spin-orbit split doublets were identified, denoted as c_0/d_0, c/d, c'/d', c''/d'', c'''/d'''.[30,31] The c_0/d_0 and c'/d' spin-orbit split are assigned to the Ce^{3+} oxidation state, while the other three spin-orbit splits are characteristic of the Ce^{4+} state. What is interesting to note is that the XPS studies can confirm a higher presence of Ce^{3+} as compared to Ce^{4+}. The O1s spectra of both samples (Figure 7d) present the main peak of the lattice oxygen signal at 530.6 eV binding energy, accompanied by small humps of surface hydroxyl groups and adsorbed water.
The Zr3d spectra (Figure 7e) displayed a strong spin-orbit doublet Zr $3d_{5/2}$-Zr $3d_{3/2}$ with splitting of 2.35 eV. It was fitted by a single component (Zr-O) with the binding energy of 181.7 ± 0.2 eV for the Zr $3d_{5/2}$ characteristic of ZrO_2 for the CeZrLa-GO sample. For the CeZrLa sample, a second phase of $Zr(OH)_4$ at 183.2 eV was observed, in agreement with the higher amount of OH found for this sample. The high resolution spectra of La 3d (Figure 7f) reveal binding energies characteristic of the 3^+ oxidation state.

In this work, the environmental impact, sustainability and carbon footprint have been evaluated by a life cycle assessment (LCA) as recommended by practitioners in the field.[32] A brief account of potential environmental and human health impacts associated with the synthesis of the starting materials used in this work are further described in Supporting Information. Thus far only a recent work by Demirel et al. deals with the topic of sustainability of PC production from PO and CO_2 via two routes using ionic liquid and a salen metal complex as an economically feasible alternative to the current industrial practice of using the highly toxic precursors bisphenol A and diphenyl carbonate.[33] Demirel et al. stress that expensive and inefficient catalysts are the main hurdles to the commercialisation of the promising CO_2 utilisation technology for producing PC and poly-PC at an industrial scale. To fully answer the question whether the CHFS of the GO-supported catalyst can be considered a "greener" alternative to conventional materials synthesis methods (such as the co-precipitation method, sol-gel and hydrothermal methods), further LCA comparison of the available methods would have to be carried out to fully assess the multifaceted environmental impact.

4. Conclusions

The exploration of graphene properties has paved the way for innovative applications and new devices. One such application is the process described herein: the direct synthesis of propylene carbonate, a valuable, industrially relevant chemical product. The synthesis route involves the utilisation of CO_2, without the use of organic solvents thereby making it significantly more environmentally sustainable. This paper reports for the first time a controllable and simple direct all-in-one 3D printing method for the manufacture of a reduced graphene oxide GO-based nanocomposite catalyst. The holistic environmental benefits of the entire CeZrLa-GO

catalyst utilisation also come from the CHFS qualifying from a sustainability perspective, *as a* "green" process with great potential for the design of novel catalyst systems such *as* CeZrLa-GO as well as any other future novel catalyst systems.

In addition, this work demonstrates that the graphene-based structure and metal oxide particle loading can be truly tailored at every level, from the fine-controlled synthesis at the nano- and micro-scale through to the reactor structure engineering at the macro-scale. The results obtained provide a significant advance on existing attempts at the 3D printing of graphene inks into 3D structures as the previous attempts merely explored the printability itself. In contrast, this study offers a practical edge towards the production of novel, high quality, on-demand, scalable structured graphene-based catalysts for bespoke design and improvement of the catalytic reactor as well as the chemical production processes. The resulting 3D printed structures exhibited higher catalytic activity than that of the starting powder even when screened only in a batch reactor. When compared to conventionally used random packed beds, the 3D structures will be highly appealing to industry for their operational advantages due to flexible geometries with a high degree of control of mixing and flow behaviour and excellent reproducibility of the reactor characteristics such as low pressure drop, and maximised heat and mass transfer resulting in overall higher catalyst performance.

These well-controlled catalyst structures combine favourable aspects of both high catalytic performance and facile separation from the reaction mixture (i.e. the ease of recovery of the catalyst and product removal post-reaction). Despite the obvious benefits to pressing environmental challenges these novel processes offer, their full potential should be further explored in the context of real world applications such as multi-channel flow reactors. Additionally, there is further scope for the exploration of their cyclic stability and catalyst regeneration steps.

List of Tables and Figures

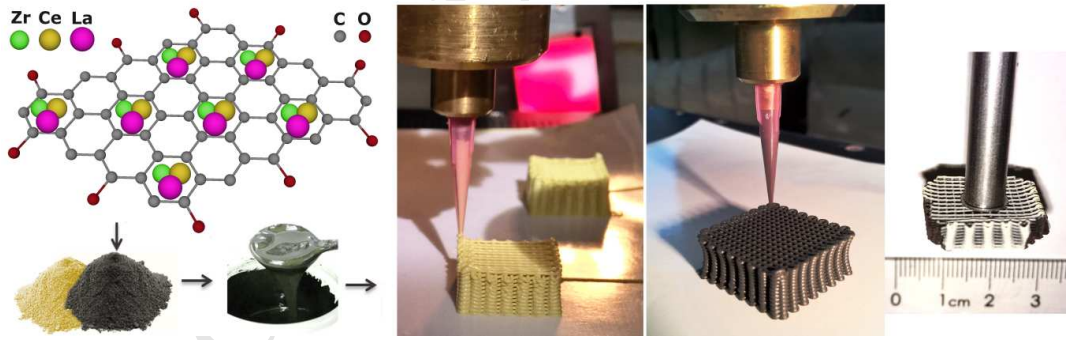

Figure 1. Process used to develop and manufacture nanocomposite structures from fine-controlled synthesis at nano- and meso-scale through the structure engineering, to the final catalyst reactor and its application: (from left to right) 2D crystal lattice model of the atomic structure of graphene-oxide and deposited mixed oxides (left), photos of 3D printing of inks both unsupported (yellow in mid-left photo) and GO-supported CeZrLa structures (grey in mid right photo), through a 600 µm nozzle in stacked layers of fibers and a typical GO-supported CeZrLa structure mounted onto an impeller shaft of a stirred batch reactor cell (right).

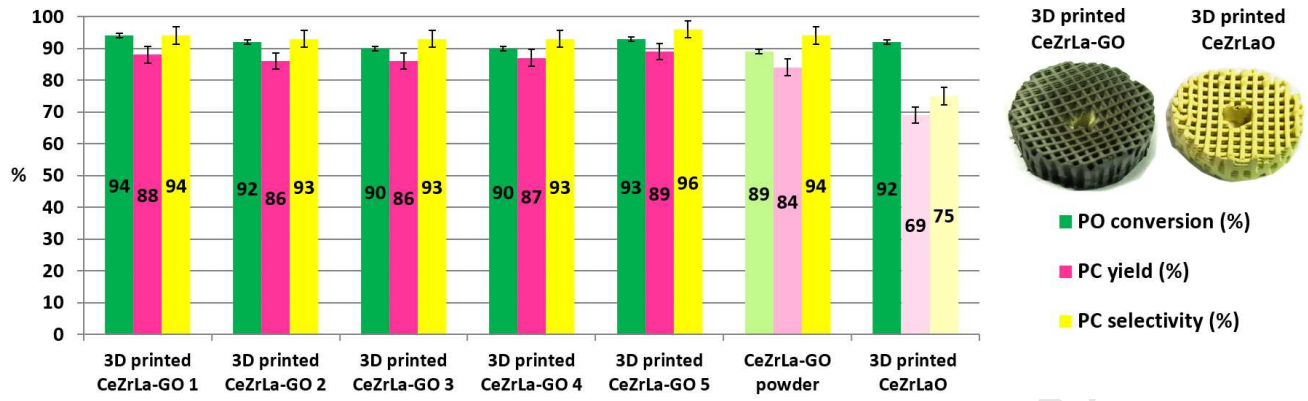

Figure 2. Results (repeatability tests) for the green synthesis of propylene carbonate using the printed graphene-supported CeZrLa catalyst (first five sets from left to right) in comparison to its powder counterpart and the printed unsupported CeZrLa catalyst (right, in lighter shades representing lower values) under optimum reaction conditions (reaction temperature 443 K, CO_2 pressure 70 bar, catalyst loading of 10% (w/w), reaction time 20 h) but with a modified stirring speed of 100 (first four runs) and 350 rpm (in the last run); the error bars, added to each column in the chart, are the standard error of the mean (see Table 1 for more detail).

Catalyst used	Catalyst loading (w/w)	Reaction time (h)	Stirring speed (rpm)	PO conversion (%)	PC yield (%)	PC selectivity (%)
3D printed CeZrLa-GO 1	10	20	100	94±2	88±1	94±1
3D printed CeZrLa-GO 2	10	20	100	92±2	86±1	93±1
3D printed CeZrLa-GO 3	10	20	100	90±2	86±1	93±1
3D printed CeZrLa-GO 4	10	20	100	90±2	87±1	93±1
3D printed CeZrLa-GO 5	10	20	350	93±2	89±1	96±1
CeZrLa-GO powder	10	20	350	89±1	84±1	94±1
3D printed CeZrLaO	10	20	100	92.0±0.5	69.0±0.5	75±1

Table 1. Summary of the evaluation of catalyst performance for 3D printed CeZrLaGO catalysts, CeZrLaGO powder and 3D printed CeZrLa catalysts: the conversion of propylene oxide, selectivity and yield of propylene carbonate are shown for operating parameters such as catalyst loading, reaction time and stirring speed. Catalyst loading is expressed here as the catalyst to reactant ratio by weight. All the measurements were performed at 443 K and at a CO_2 pressure of 70 bar.

Catalyst	BJH method: desorption surface area (m^2/g)	Pore volume (cm^3/g)	Pore radius (Å)	BET method: surface area (m^2/g)	Particle size (HRTEM) (nm)	Particle size (XRD) (nm)
CeZrLa-GO as-synthesized powder heat-treated at 500°C	-	0.04	10	92	5.4 ± 1.4 *	7.1±0.6 **
3D printed CeZrLa-GO heat-treated at 500°C before reaction	130	0.32	59	128	9.4 ± 1.5	7.2±0.5
3D printed CeZrLa-GO (heat-treated) after reaction	98	0.23	48	81	9.3 ± 1.7	7.3±0.5
3D printed CeZrLaO heat-treated at 500°C	103	0.25	59	109	9.4 ±1.8	7.1±0.6

Table 2. Measured specific surface area, pore size distribution for 3D printed nanocomposite samples including the CeZrLa-GO catalyst tested in propylene carbonate synthesis (particle size data for CeZrLa-GO powder and 3D printed structures were obtained using different instruments; for the former a JEOL 2100FCs was used for TEM analysis* and a Stoe StadiP powder diffractometer was used for XRD analysis**, as described by Adeleye et al., 2015). Pore size distribution (PSD) plots are presented in Supporting Information; additionally see Table S3 in Supplementary Information for further details on the particle size range derived from the Scherrer equation.

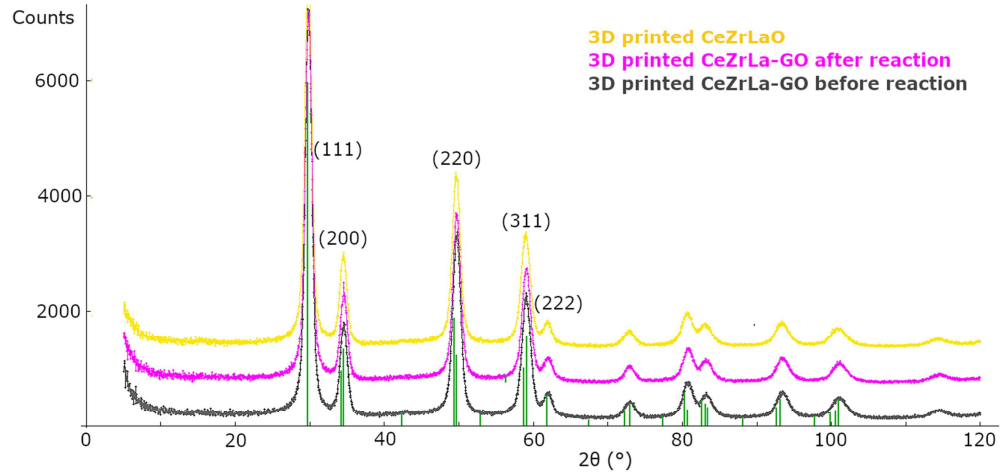

Figure 3. XRD patterns of CeZrLa and CeZrLa-GO catalysts conducted on a Philips/Panalytical X'Pert Pro diffractometer using copper Kα radiation (λ =1.541838 Å), a voltage of 40 kV and a current of 40 mA, at room temperature from 2 to 100°C 2θ (with a step size of 0.04° and a time of 4 seconds per step). Peaks can be assigned to both cubic and tetragonal CeLa- and CeZr- oxide phases (respectively) both before and after reaction (the main reflections (111), (200), (220) and (311) are observed at 29.8°, 34.5°, 49.7° and 59.0° respectively). The XRD data show that no phase change in the printed material occurred during the thermal treatment and the catalyst reaction. Rietveld refined lattice parameters and additional temperature dependent XRD analysis for the two phases are presented in Tables S2 and S3.

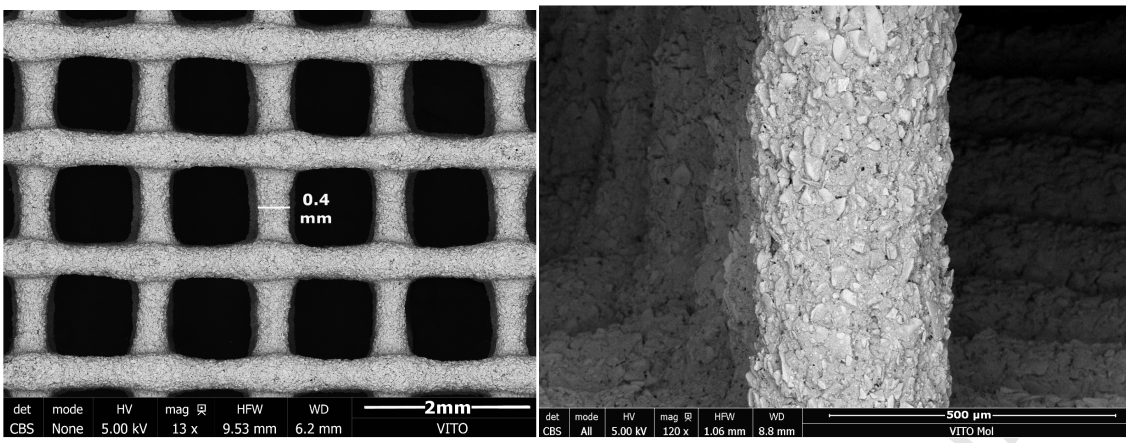

Figure 4. SEM images of a representative 3D printed CeZrLa-GO structure with a fibre thickness of 400 µm.

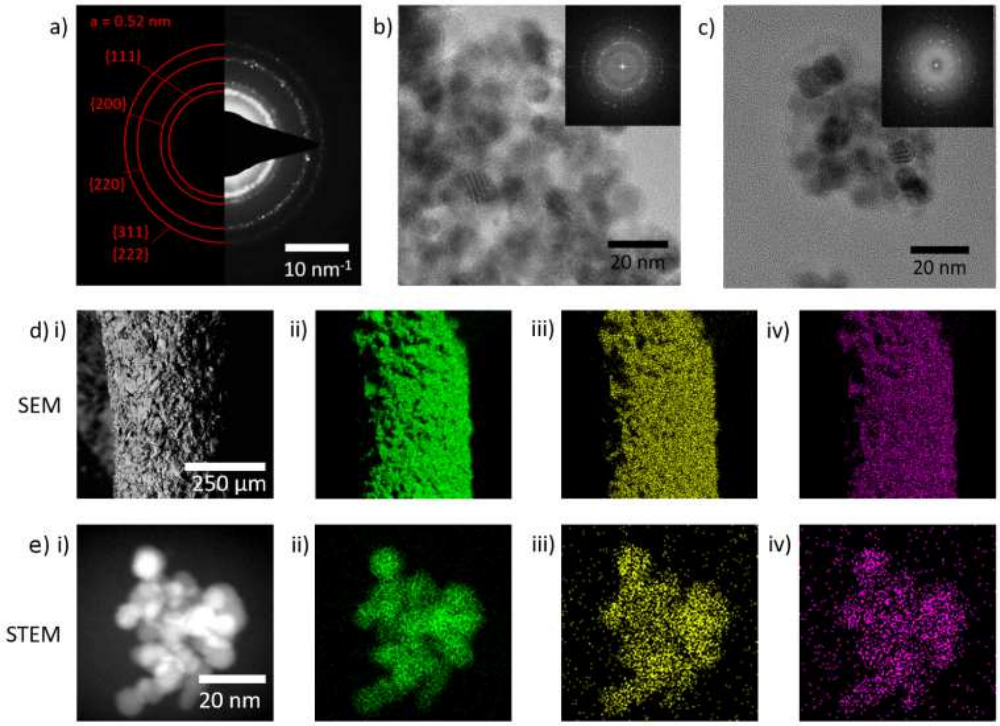

Figure 5. TEM analysis of $CeZeLaO_x$-GO nanoparticles: a) selected area diffraction pattern of nanoparticles with the associated polycrystalline rings of cubic zirconia marked. b-c) HRTEM images with inset FFTs (b) $CeZeLaO_x$ with GO before and (c) $CeZeLaO_x$ with GO after use in reaction. There is no discernible change in particle size or crystal lattice between the three samples investigated. Elemental mapping of printed structures. d) Secondary electron image (i) and associated EDX elemental maps of ii) Zr, iii) Ce and iv) La of printed $CeZrLaO_x$ with GO; d) HAADF-STEM image (i) and associated EDX elemental maps of ii) Zr, iii) Ce and iv) La of printed $CeZrLaO_x$ with GO. The chemistry of the sample is homogeneous at the macro and nano-scales**.**

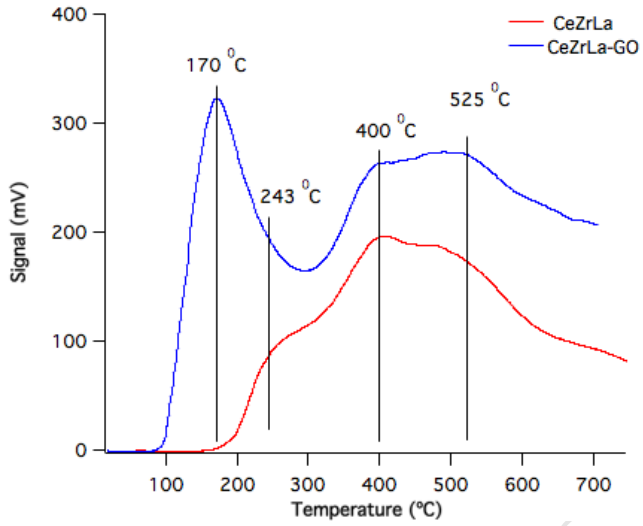

Figure 6. NH_3-TPD profiles of printed CeZrLa and CeZrLa-GO materials

Catalyst sample	T_{des} (°C)	NH_3 uptake ($\mu mol.g^{-1}$)
3D printed CeZrLa	243	118.8
	400	287.7
	525	551.4
3D printed CeZrLa-GO	170	408.7
	400	454.9
	525	329.3

Table 3. Temperature programmed desorption of NH_3 for CeZrLa and CeZrLa-GO samples

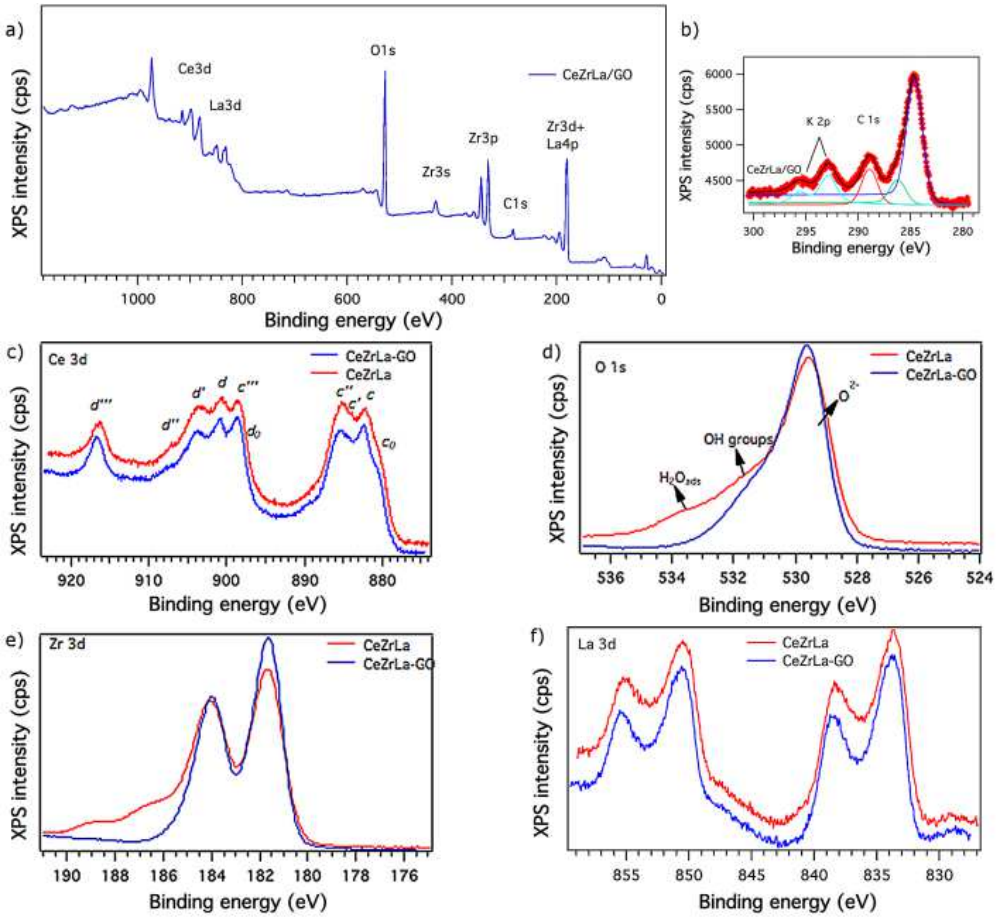

Figure 7. Wide XPS spectra for CeZrLa-GO printed sample (a). C1s and K2p XPS spectra for CeZrLa-GO printed sample (b). Comparison of high resolution spectra for Ce 3d(c), O1s (d), Zr3d (f) and La3d (g) in GO- containing and GO-free printed samples.

ACKNOWLEDGMENTS

SK and BS would like to thank the EPSRC Grand Challenge Network, the CO_2Chem for Seedcorn Grant (2016). TS would like to acknowledge HEFCE funding through the UK Research Partnership Investment Funding (UKRPIF) Manchester RPIF Round 2 for the Multiscale Characterisation Facility at The University of Manchester. The authors would like to acknowledge the contribution of Dr. T. L. Burnett who provided access to Electron Microscopy facilities at University of Manchester and their respective institutions for the financial support provided. All the authors also gratefully acknowledge the financial support provided by their respective institutions.

ABBREVIATIONS

Reduced graphene oxide - GO; Continuous Hydrothermal Flow Synthesis - CHFS; Barrett-Joyner-Halenda - BJH; Brunauer-Emmett-Teller - BET; transmission electron microscopy - TEM; selected area electron diffraction – SAED; high angle annular dark field – HAADF; energy dispersive X-ray – EDX; scanning transmission electron microscopy – STEM; scanning electron microscope – SEM; Fast Fourier Transform (FFT), Thermogravimetric and differential thermogravimetric analyses – TGA/DTG; Temperature programmed desorption - TPD, X-ray photoelectron spectroscopy – XPS; propylene oxide -PO; propylene carbonate - PC.

Supporting Information Paragraph

This section contains further details regarding the characterisation of the printed structures carried out using TGA-DTG, XRD, TEM, SEM and STEM accompanied by compositional EDX analysis. In addition, the Supporting Information section presents some preliminary results on life cycle assessment (LCA) of the CHFS of the CeZrLa-GO material.

REFERENCES

1. N. Yang, R. Wang, Sustainable technologies for the reclamation of greenhouse gas CO_2. Journal of Cleaner Production, **2015**,103, 784.
2. R. Wennersten, Q. Sun, H. Li, The future potential for Carbon Capture and Storage in climate change mitigation – an overview from perspectives of technology, economy and risk. Journal of Cleaner Production, **2015**, 103. 724.
3. S. Fujita M. Arai, B.M. Bhanage (eds.), Direct transformation of carbon dioxide to value-added products over heterogeneous catalysts, transformation and utilization of carbon dioxide. Green Chemistry and Sustainable Technology, Springer-Verlag, **2014**.
4. (a) A. I. Adeleye, D. Patel, D. Niyogi, B. Saha, Efficient and Greener Synthesis of Propylene Carbonate from Carbon Dioxide and Propylene Oxide, Ind. Eng. Chem. Res., **2014**, 53, 18647 (b) A.I. Adeleye, S. Kellici, T. Heil, D. Morgan, M. Vickers, B. Saha, Greener synthesis of propylene carbonate using graphene-inorganic nanocomposite catalysts. Catal. Today, **2015,** 256(2), 347.
5. W.F. Monteiro, M.O. Vieira, A.S. Aquino, M.O. de Souza, J. Lima, S. Einloft, R. Ligabue, CO_2 conversion to propylene carbonate catalyzed by ionic liquid containing organosilane groups supported on titanate nanotubes/nanowires. Applied Catalysis A: General, **2017**, 544, 46.
6. J. Peng, H-J. Yang, Y. Geng, Z. Wei, L. Wang, C-Y. Guo, Novel, recyclable supramolecular metal complexes for the synthesis of cyclic carbonates from epoxides and CO_2 under solvent-free conditions, Journal of CO_2 utilization, **2017**, 17, 243.
7. M. North, R. Pasquale, C. Young, Synthesis of cyclic carbonates from epoxides and CO_2. Green Chemistry, **2010**,12, 1514.
8. Q. Tang, Z. Zhen Zho, Z. Chen, Graphene-related nanomaterials: tuning properties by functionalization. Nanoscale, **2013**, 5, 4541.
9. A.E. Jakus, E.B. Secor, A.L. Rutz, S.W. Jordan, M.C. Hersam, R.N. Shah, Three-dimensional printing of high-content graphene scaffolds for electronic and biomedical applications. ACS Nano **2015,** 9(4), 4636.
10. D. Lin, S. Jin, F. Zhang, C. Wang, Y. Wang, C. Zhou, G.J. Cheng, 3D stereolithography printing of graphene oxide reinforced complex architectures. Nanotechnol **2015**, 26, 434003.
11. C. Zhu, T. Yong-Jin Han, E.B. Duoss, A.M. Golobic, J.D. Kuntz, C.M. Spadaccini, M.A. Worsley, Highly compressible 3D periodic graphene aerogel microlattices. Nat Commun **2015**, 6, 6962.
12. C.R. Tubío, A. Rama, M. Gómez, F. del Río, F. Guitián, A. Gil, 3D-printed graphene-Al_2O_3 composites with complex mesoscale architecture, Ceramics International. **2018**, 44, 5760
13. V. Georgakilas, J.N. Tiwari, K.C. Kemp, J.A. Perman, A.B. Bourlinos, K.S. Kim, R. Zboril, Noncovalent functionalization of graphene and graphene oxide for energy materials, biosensing, catalytic, and biomedical applications. Chem Rev **2016**, 116(9), 5464.

14. E. García-Tuñon, S. Barg, J. Franco, R. Bell, S. Eslava, E. D'Elia, R.C. Maher, F. Guitian, E. Saiz, Printing in three dimensions with graphene. Adv Mater **2015**, 27, *1688.*
15. Q. Zhang, F. Zhang, S.P. Medarametla, H. Li, C. Zhou, D. Lin, 3D Printing of Graphene Aerogels. Small **2016**, 12 (13), 1702.
16. J. Azuaje, C.R Tubío, L. Escalante, M. Gómez, F. Guitián, A. Coelho, O. Caamaño, A. Gil, E. Sotelo, An efficient and recyclable 3D printed α-Al_2O_3 catalyst for the multicomponent assembly of bioactive heterocycles. Appl Catal A **2017**, 530, 203.
17. C.R Tubío, J. Azuaje, L. Escalante, A. Coelho, F. Guitián, E. Sotelo, A. Gil, 3D printing of a heterogeneous copper-based catalyst. J Catal 2**016**, 334, 110
18. J. Lefevere, M. Gysen, S. Mullens, V. Meynen, J. Van Noyen, J The benefit of design of support architectures for zeolite coated structured catalysts for methanol-to-olefin conversion. Catal Today **2013**, 216, 18
19. S. Danaci, L. Protasova, F. Snijkers, W. Bouwen, A. Bengaouer, P. Marty, Innovative 3D-manufacture of structured copper supports post-coated with catalytic material for CO_2 methanation. Chemical Engineering and Processing **2018**, 127, 168
20. V. Middelkoop, K. Coenen. J. Schalck, M. Van Sint Annaland, F. Gallucci, 3D printed versus spherical adsorbents for gas sweetening. Chemical Engineering Journal 2019, 357, 309
21. (a) S. Kellici, J. Acord, K.E. Moore, N.P. Power, V. Middelkoop, D.J. Morgan, T. Heil, P. Coppo, I.-A. Baragaua and C.L. Raston, Continuous hydrothermal flow synthesis of graphene quantum dots. React. Chem. Eng. **2018**,3, 949-958 (b) V. Middelkoop, C.J. Tighe, S. Kellici, R.I. Gruar, J.M. Perkins, S.D.M. Jacques, P. Barnes, J. Darr, Imaging the continuous hydrothermal flow synthesis of nanoparticulate CeO_2 at different supercritical water temperatures using in situ angle-dispersive diffraction. J Supercrit Fluids, **2014**, 87, 118.
22. W-L. Dai, S-F. Yin, R. Guo, S-L. Luo, X. Du, C.-T. Au, Synthesis of propylene carbonate from carbon dioxide and propylene oxide using Zn-Mg-Al composite oxide as high-efficiency catalyst. Catal. Lett. **2010**, 136, 35.
23. R. Srinivasan, R.J. De Angelis, G. Ice, B.H. Davis, Identification of tetragonal and cubic structures of zirconia using synchrotron x-radiation source. J. Mater. Res. **1991**, *6*, 1287-1292
24. J. Lian, J. Zhang, F. Namavar, Y. Zhang, F. Lu, H. Haider, K. Garvin, W.J. Weber, R.C. Ewing, Ion beam-induced amorphous-to-tetragonal phase transformation and grain growth of nanocrystalline zirconia. Nanotechnology **2009**, 20, 245303.
25. W.E. Farneth, R.J. Gorte, Methods for Characterizing Zeolite Acidity. Chem. Rev. **1995,** 95, 615.
26. (a) A. Primo, F. Neatu, M. Florea, V. Parvulescu, H. Garcia, Graphenes in the absence of metals as carbocatalysts for selective acetylene hydrogenation and alkene hydrogenation. Nature Communications, **2014,** 5, 5291; (b) G. Bian, P. Jiang, W. Zhang, K. Jiang, L. Hu, Z. Jian, Y. Shena, P. Zhang, A novel poly(p-styrenesulfonic acid) grafted carbon nanotube/graphene oxide architecture with enhanced catalytic performance for the synthesis of benzoate esters and fatty acid alkyl esters. RSC Advances, 2015, 5(110), 90757-90765.
27. G. Xie, Z. Liu, Z. Zhu, Q. Liu, J. Ge, Z. Huang, Simultaneous removal of SO_2 and NO_x from flue gas using a CuO/Al_2O_3 catalyst sorbent II. Promotion of SCR activity by SO_2 at high temperatures. Catal. **2004**, 224, 42.
28. R.Q. Long, R.T. Yang, Characterization of Fe-ZSM-5 Catalyst for Selective Catalytic Reduction of Nitric Oxide by Ammonia. J. Catal. **2000**, 194, 80.
29. B. Li, L. Zhang, Y. Song, D. Bai, H. Jing, Brønsted acid improved cycloaddition of carbon dioxide to propylene oxide. Journal of Molecular Catalysis A: Chemical. **2012**, 363–364, 26.
30. H. Borchert, Y.V. Frolova, V.V. Kaichev, I.P. Prosvirin, G.M. Alikina, A.I. Lukashevich, V.I. Zaikovskii, E.M. Moroz, S.N. Trukhan, V.P. Ivanov, E.A. Paukshtis, V.I. Bukhtiyarov, V.A. Sadykov, Electronic and chemical properties of nanostructured cerium dioxide doped with praseodymium. Journal of Physical Chemistry B, **2005**, 109, 5728.
31. F. Zhang, P. Wang, J. Koberstein, S. Khalid, S.W. Chan, Cerium oxidation state in ceria nanoparticles studied with X-ray photoelectron spectroscopy and absorption near edge spectroscopy. Surface Science, **2004,** 563, 74.
32. L. Čuček, J, J. Klemeš, Z. Kravanja, A Review of footprint analysis tools for monitoring impacts on sustainability, Journal of Cleaner Production, 2012, 34, 9.
33. Y. Demirel Sustainability and economic analysis of propylene carbonate and polypropylene carbonate production processes using CO_2 and propylene oxide, J Chem Eng Process Technol 2015, 6, 1000236

Catalyst used	Catalyst loading (w/w)	Reaction time (h)	Stirring speed (rpm)	PO conversion (%)	PC yield (%)	PC selectivity (%)
3D printed CeZrLa-GO 1	10	20	100	94±2	88±1	94±1
3D printed CeZrLa-GO 2	10	20	100	92±2	86±1	93±1
3D printed CeZrLa-GO 3	10	20	100	90±2	86±1	93±1
3D printed CeZrLa-GO 4	10	20	100	90±2	87±1	93±1
3D printed CeZrLa-GO 5	10	20	350	93±2	89±1	96±1
CeZrLa-GO powder	10	20	350	89±1	84±1	94±1
3D printed CeZrLaO	10	20	100	92.0±0.5	69.0±0.5	75±1

Table 1.

Catalyst	BJH method: desorption surface area (m^2/g)	Pore volume (cm^3/g)	Pore radius (Å)	BET method: surface area (m^2/g)	Particle size (HRTEM) (nm)	Particle size (XRD) (nm)
CeZrLa-GO as-synthesized powder heat-treated at 500°C	-	0.04	10	92	5.4 ± 1.4 *	7.1±0.6 **
3D printed CeZrLa-GO heat-treated at 500°C before reaction	130	0.32	59	128	9.4 ± 1.5	7.2±0.5
3D printed CeZrLa-GO (heat-treated) after reaction	98	0.23	48	81	9.3 ± 1.7	7.3±0.5
3D printed CeZrLaO heat-treated at 500°C	103	0.25	59	109	9.4 ±1.8	7.1±0.6

Table 2.

Catalyst sample	T_{des} (°C)	NH_3 uptake ($\mu mol.g^{-1}$)
3D printed CeZrLaO	243	118.8
	400	287.7
	525	551.4
3D printed CeZrLa-GO	170	408.7
	400	454.9
	525	329.3

Table 3.

- studies of 3D printed Ce-La-Zr GO catalyst performance in CO_2 utilisation reaction
- highly active Ce-La-Zr graphene oxide nanocomposite catalyst synthesised using CHFS
- CHFS-continuous hydrothermal flow synthesis: controlled, rapid and efficient route
- direct synthesis of propylene carbonate in the absence of organic solvents
- improved catalytic activity of well-controlled 3D printed Ce-La-Zr-GO catalysts